Design of Compressor Impellers for Water as a Refrigerant

Norbert Müller, Ph.D.

ABSTRACT

This paper introduces a design procedure for a compressor system with separately driven pre-runner and main runner. The approach is restricted to radial-line blading, generally used for high work transmission, high-volume flows, and/or for reasons of stability and technology. Initially the intended application was the compression of water vapor under a vacuum condition with a high-pressure ratio for use in an environmental friendly refrigeration plant with water as a refrigerant.

The paper introduces some geometrical aspects of radial-line blading. It gives an algorithm for a quick design and flow calculation of a wheel pair consisting of pre-runner and main runner, where the pre-runner is axial with curved blades and the main runner is mixed-flow with totally straight blades. A design example is shown along with examination of flow stability and design rules for such a system.

INTRODUCTION

Water is a natural refrigerant. It is absolutely harmless to man and nature. It is easily available, and there are no problems disposing it after use. Even though water is one of the oldest refrigerants, it requires state-of-the-art technology to use water as a refrigerant in absorption chillers or in compression chillers with steam injection compressors. These techniques are energy efficient as long as there is waste heat or steam available. However, higher energy efficiency can be achieved using compression refrigeration plants with turbo compressors. Successful applications of such plants have occurred as recently as just a few years ago.

Water as a refrigerant has some specific features that complicate its application in refrigeration plants with turbo compressors (Albring and Müller 1995). Since the cycle works under coarse vacuum, the volumetric cooling capacity of water vapor is very low and huge volume flows have to be compressed with relatively high pressure ratios. So, compared with classical refrigerants such as R-134a or R-12, the use of water (R-718) as a refrigerant causes approximately a 200 times higher volume flow and a double pressure ratio for the same application. Due to the thermodynamic properties of water vapor, this high pressure ratio requires a circumferential speed approximately 2 to 4 times higher, depending on the impeller design, while the speed of sound is approximately 2.5 times higher. Reynolds numbers are about 300 times lower, and the specific work transmission per unit mass has to be around 15 times higher. High-performance mixed-flow turbo compressors are especially suitable for this task (Albring et al. 1998).

High pressure ratios can be obtained using these compressors by a combination of high rpm and large diameter, where the diameter is primarily limited by the available space and manufacturing facility. When compressing water vapor, the tip speed is often limited by the rotor stability rather than by the speed of sound. Working under vacuum, the forces exerted by the gas on the blades are very small, so the blades must largely withstand centrifugal forces resulting from their inherent mass. Hence, lightweight construction is used with extremely thin, mostly straight blades made of titanium or composite material sheets. These impellers cannot be milled. Generally they are built of several parts (Albring et al. 1994) and are different from the usual high-performance impellers.

Since the blade angle is uniformly 90 degrees, a guiding device is needed to prevent high incidence losses. Using a stator is the simplest solution, but this is associated with

Norbert Müller carried out the documented work in the Department of Mechanical Engineering, Technische Universität, Dresden, Germany. He is now a post-doctoral research scientist and adjunct associate professor in the Department of Mechanical Engineering, Columbia University, New York.

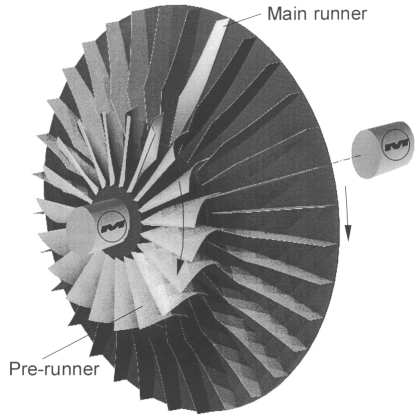

Figure 1 *Pre-runner and main runner.*

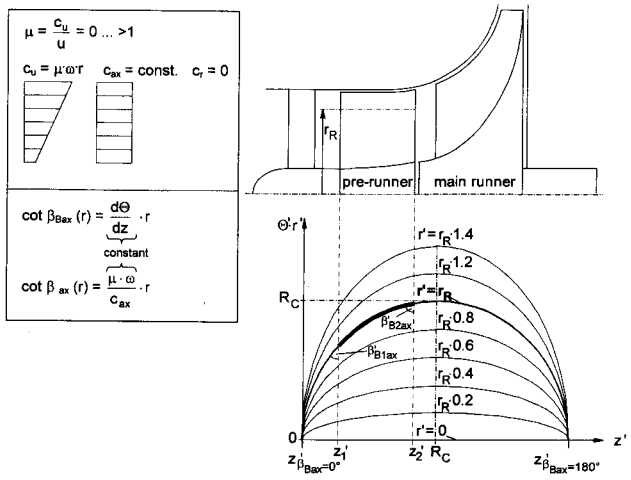

Figure 2 *Radial-line blading.*

reduced work transmission in the rotor. An inducer with curved blades on the same shaft allows a higher work transmission. It usually has a smaller diameter, and, therefore, its tip speed does not reach the limit possible by today's high-strength materials. So in order to obtain an even higher work transmission, the inducer can be cut off the main shaft and driven separately at the highest rpm allowable by stability or Mach number limit considerations.

In the following, the separated inducer is called a *pre-runner* and the following mixed-flow impeller is called the *main runner.* Both impellers rotate in the same direction, and there are no guide vanes between them. Due to high centrifugal forces and for technological reasons, both impellers have radial-line blading (Figure 1).

Radial line blading produces a solid-body-like rotation, so that most methods for free vortex design are not appropriate for such a system. In this study, a fast, quasi-three-dimensional algorithm for the preliminary design and flow calculation of such a system is introduced. A design example shows that a reasonable design of such a system can be achieved. Some investigations of flow stability in such a system with radial line blading are included. Also, design rules for the maximization of work transmission are derived by applying Euler's equation to a mean line model, since high-pressure ratios are desired for the application.

RESEARCH

Radial-Line Blading

The blades of the pre-runner are curved in order to produce the necessary pre-swirl for the main runner with totally straight blades. A given camber line at reference radius r_R determines the camber surface of the pre-runner blading since radial-line blading is used. Here a circular arc forms the camber line at r_R (Figure 2). Such a blading is very suitable for velocities close to the speed of sound (Traupel 1988) and at low Reynolds numbers (Schmitz 1960).

Giving the axial blade angle at leading and trailing edge $\beta_{Bax1}'(r_R)$ and $\beta_{Bax2}'(r_R)$ and the axial length of the pre-runner $L'_{ax} = z_2' - z_1'$ determines the camber line at r_R:

$$\beta_{Bax}'(z',r_R) = \arccos\left(\frac{(z_2' - z')\cdot\cos\beta'_{Bax1}(r_R) + (z' - z_1')\cdot\cos\beta'_{Bax2}(r_R)}{z_2' - z_1'}\right) \quad (1)$$

$$\Theta'(z') = \frac{z_2' - z'}{r_R}\cdot\cot\left(\frac{\beta'_{Bax}(z',r_R) + \beta'_{Bax2}(r_R)}{2}\right) \quad (2)$$

Using radial-line blading $\beta_{Bax}'(z', r_R)$ determines $\beta_{Bax}'(z', r')$ at any location (z', r'); also, if the camber line at r_R is not a circular arc,

$$\beta_{Bax}'(z',r') = \operatorname{arccot}\left(\frac{r'}{r_R}\cdot\cot\beta'_{Bax}(z',r_R)\right) \quad (3)$$

If the camber line at r_R is a circular arc with radius R_C, at all other radii r' it is an elliptic arc with the semiaxis R_C in the z direction. The semiaxis in the Θ direction is less than R_C at $r' < r_R$ and always greater than R_C at $r' > r_R$ (Figure 2). Depending on the specific design with $\beta_{Bax1}'(r_R) > 0$ and $\beta_{Bax2}'(r_R) < 180°$, only a section of the arc applies to the blading.

Also, the flow angle $\beta(r)$ follows Equation 3, assuming a solid-body swirl distribution and axial flow with $c_m(r)$ = constant (see Figure 2 on the left). Hence, $\beta(r_R) = \beta_B(r_R)$ and also $\beta(r) = \beta_B(r)$ are true for any radius $r \neq r_R$. Applying that to the pre-runner implies that if the flow and blade angle once match at leading and trailing edge, a change of reference radius r_R will not alter the matching, but it does alter the derivations $\partial\beta_B'/\partial r'$ and $\partial\beta_B'/\partial z'$. So changing r_R is a means to altering the load distribution on the blades (Figure 3).

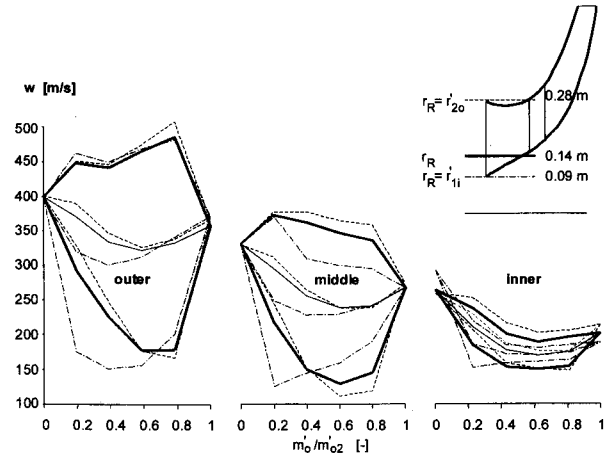

Figure 3 *Change of reference radius changes load distribution.*

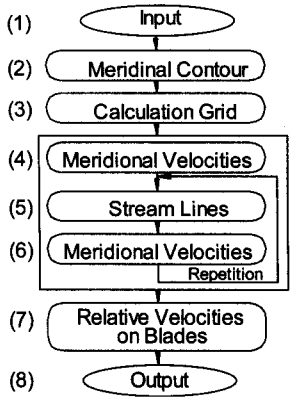

Figure 4 *Algorithm flow chart.*

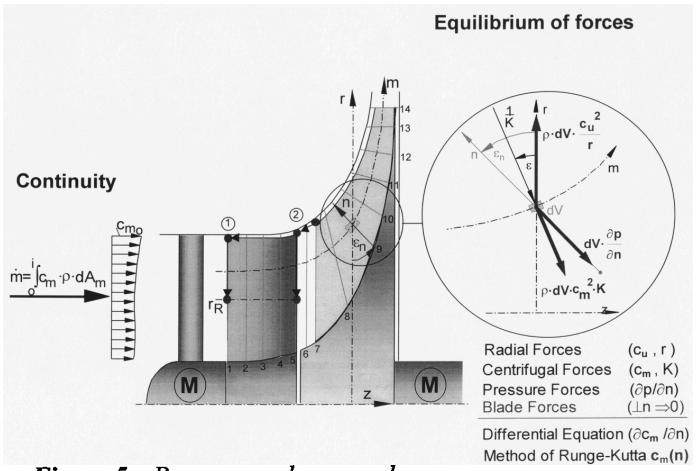

Figure 5 *Programmed approach.*

The blade thickness at the pre-runner is determined by giving a thickness at the outer diameter δ_{Bo}' and an inward increase of thickness, $d\delta_B'/dr$. The blade thickness of the main runner blades δ_B is constant.

Algorithm

The algorithm is a quick design method for the pre-runner and main runner, as well as a flow calculation method for off-design points. It is meant for subsonic use of the impellers. It is also stable at transonic and supersonic velocities, but supersonic shocks are ignored. Losses due to viscous effects, flow separation, incidence, and supersonic shocks are introduced by means of estimated efficiency coefficients for both impellers.

The algorithm (Figure 4) is primarily based on the simple equilibrium of forces and the satisfaction of continuity (Figure 5). In this quasi-three-dimensional code, a blade-to-blade flow calculation is superimposed on a two-dimensional through-flow calculation to obtain the velocity distribution on the impeller blades. The geometric generator for the pre-runner blading is connected to the flow calculation, which leads to the desired incidences for both impellers.

Simple Equilibrium of Forces. The equilibrium of the following forces is considered: (1) radial force due to circumferential velocity component of the fluid, (2) centrifugal force due to curvature of the meridional streamlines and meridional velocity component of the fluid, (3) pressure force due to the pressure gradient, and (4) blade force, exerted on the fluid. The equilibrium is in the n direction according to Figure 5.

In the pre-runner region, where the blades are curved, the n direction corresponds to the radial direction. Everywhere else, where there are no blades or the blades have a constant angle of 90°, the n direction can be in any direction. Consequently, the blade force is zero or has no component in the n direction because the blade force is normal to the blade surface, e.g., in the circumferential direction, when using radial-line blades.

After substituting $\partial p(n)/\partial n/\rho(n)$ by $\partial h_t(n)/\partial n - \partial c(n)^2/\partial n\,/2$ and considering $c(n)^2 = c_u(n)^2 + c_m(n)^2$, the differential Equation 4 for the meridional velocity can be obtained from the equilibrium in Figure 5.

$$\frac{\partial c_m(n)}{\partial n} = c_m(n)\cdot K(n)\cdot\cos(\varepsilon_n - \varepsilon(n)) + \frac{\frac{\partial h_t(n)}{\partial(n)} - c_u(n)\cdot\frac{\partial c_u(n)}{\partial(n)} - \frac{c_u(n)^2}{r(n)}\cdot\cos(\varepsilon_n)}{c_m(n)} \quad (4)$$

Equation 4 applies when $c_u(n)$ and $h_t(n)$ are known, as is the case in a vaneless region, where constant angular momentum is assumed. For a known flow angle $\beta(n)$, the term $\omega\cdot r(n) - \cot\beta(n)\cdot c_m(n)$ replaces $c_u(n)$. Considering that $\cos(\varepsilon_n) = \partial r(n)/\partial n$, Equation 5 is obtained. Equation 5 applies for most impeller regions.

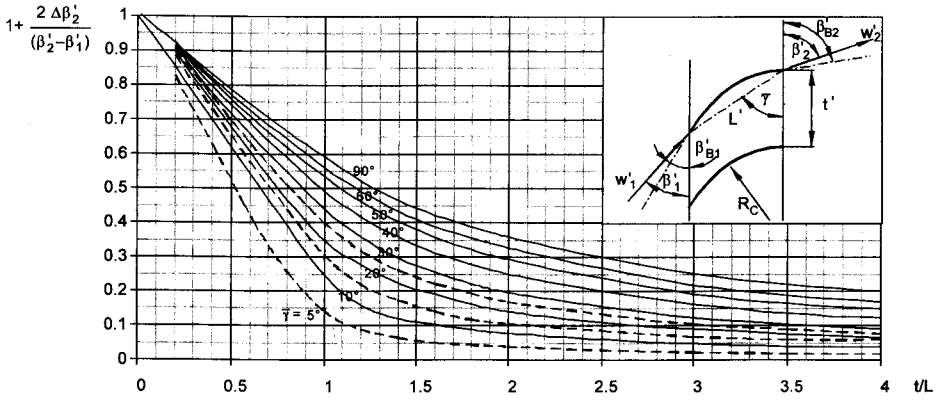

Figure 6 *Deviation angle: exaggeration factor after Weinig (1935).*

$$\frac{\partial c_m(n)}{\partial n} = \frac{\left(\begin{array}{l} c_m(n) \cdot \left(K(n) \cdot \cos(\varepsilon_n - \varepsilon(n)) - \dfrac{\cot^2\beta(n) \cdot \cos(\varepsilon_n)}{r(n)} \right. \\ \left. -\cot\beta(n) \cdot \dfrac{\partial \cot\beta(n)}{\partial n} \right) + \\ \dfrac{\dfrac{\partial h_{t1}(n)}{\partial(n)} - \omega \cdot \left(\dfrac{\partial(r_1 c_{u1}(n))}{\partial n} \right)}{c_m(n)} + 2\omega \cdot \cot\beta(n) \cdot \cos(\varepsilon_n) \end{array} \right)}{1 + \cot^2\beta(n)} \tag{5}$$

Deviation Coefficient Main Runner Outlet. The Stanitz radius before the outlet of the mixed flow impeller, where the flow angle begins to deviate from the blade angle, gives Equation 6 after Stanitz and Prian (1951).

$$r_s = r_2 \cdot \exp\left(-0.71 \cdot \frac{2\pi}{N}\right) \tag{6}$$

Since the blades of the main runner have a constant blade angle of 90°, the deviation coefficient is here defined as $\mu = c_u/u$. For $\beta_{B2} = 90°$, results of Busemann (1928) and the recommendation of Traupel (1988) suggest the use of Equation 7 for prediction.

$$\begin{aligned} \mu_{2,N=16} &= 0.85 && for \frac{D_1}{D_2} \le 0.65 \\ &= 5.778 \cdot \frac{D_1}{D_2} - 4.444 \cdot \left(\frac{D_1}{D_2}\right)^2 - 1.028 && for \frac{D_1}{D_2} > 0.65 \\ \mu_2 &= 1 - (1 - \mu_{2,N=16}) \cdot \frac{16}{N} \end{aligned} \tag{7}$$

A quadratic formulation for $\mu(r)$ in the region $r_S < r < r_2$ and for β_B = constant = 90° results in Equation 8.

$$\mu(r) = \mu_2 \cdot \frac{(r - r_s)^2 + 2r_s \cdot (r - r_s) + r_2^2 - r^2}{(r_s - r_2)^2} \qquad for\ r_s < r < r_2 \tag{8}$$

TABLE 1
Necessary Input

Necessary Input Values		Symbol
Fluid	Gas constant	G
	Isentropic exponent	κ
Suction condition	Total suction pressure	p_{t1}'
	Total suction temperature	T_{t1}'
Operating point	Suction volume flow	$\dot{V}_{t1}'$
	Tip speed	$u_{o\,max}', u_2$
	Efficiency coefficient	η', η
Meridional contour	Outer diameter	$D_{1o}', D_{2o}', D_{1o}, D_2$
	Inner diameter	D_{1i}', D_{2i}', D_{1i}
	Axial position of leading and trailing edge	$z_1', z_2', z_1, z_{2o}, z_{2i}$
Blading	Blade number	N', N
	Blade thickness	$\delta_{Bo}', d\delta_B'/dr, \delta_B$

It was shown by Müller (1999) that Equation 8 is equivalent to the quadratic formulation for sin(β(r)) (Stanitz and Prian 1951) or cos(β(r)) (Traupel 1988) for β_B = constant = 90°. In the approach chosen here, $c_u(r)$ results directly from $u(r)$. So the calculation is independent of the meridional component, simplifying the algorithm, and Equation 4 can also be used in the region $r_S \le r \le r_2$.

Deviation Angle Pre-Runner Outlet. The necessary exaggeration of the blade angle at the pre-runner outlet $\Delta\beta_2'$ is predicted as a suggested value from a digitized plot after Weinig (1935) and Traupel (1988), shown in Figure 6. After Traupel (1988) this approach also gives surprisingly good results if the blades do not have an exact arc profile.

Incidence Angle Pre-Runner Inlet. According to Weinig (1935) the optimal incidence angle has a magnitude

TABLE 2
Optional Input

Suggested Values for Blading			Default Value
Pre-runner	Deviation angle	$\Delta\beta_{2o}'$	Figure 6
		$\Delta\beta_{2i}'$	Figure 6
	Axial blade angle at reference radius	$\beta_{B1ax}'(r_R)^{\#}$	for $\iota_o' = -\Delta\beta_{2o}'$
		$\beta_{B2ax}'(r_R)$	for $\iota_o' = 0$
	Reference radius	r_R	r_{2o}
Main runner	Deviation coefficient	μ_2	Equation 7

$^{\#}\iota_o'$ can be used alternatively

equal to that of the deviation angle at the outlet. So the incidence angle is suggested to be $\iota' = -\Delta\beta_2'$. Using radial line blading, it can be given only at one radius. It is given at the outer radius, since the highest work transmission occurs there.

Incidence Angle Main Runner Inlet. Following Lieblein (1965) the optimal incidence angle for $\beta_1 = 90°$ is positive and close to zero. Considering the compressibility after Wennerstrom (1965) for $\beta_2 - \beta_1 \approx 0$, that value shifts to 2 ... 3° at Mach number $M_{w1} \approx 0.7$. So as default, an incidence angle at the outer radius of $\iota_o = 0$ is used.

Programmed Code. Figure 4 shows a flow chart of the programmed code.

1. *Input.* To ease the designer's work, the algorithm requires as few as possible input values (Table 1) for a preliminary design of matching pre-runner and main runner. Changing the default values of the optional inputs (Table 2), the designer can diversify the design according to his or her own judgment.

2. *Meridional contour.* The meridional contour is an interpolating Bezier curve (Farin 1993) at the inner and outer diameter. It results from the input coordinates (z, D) at the inner and outer diameter of the leading and trailing edges of both impellers. The Bezier curve determines the coordinates (z, r) as well as the inclination $\varepsilon(m)$ and curvature $K(m)$ everywhere at the inner and outer diameter.

3. *Calculation grid.* Leading and trailing edges partition the curve, as does the Stanitz radius for the part of the main runner. The curve segments in the region of the main runner are then subdivided by equal parameter length. At the pre-runner and between the impellers, equal axial lengths subdivide the curves. Lines connect points of the same number at the inner and outer diameter and serve as calculating gridlines in the n direction. The m gridlines—the meridional streamlines—connect equal numbered points at the n gridlines. For the first calculation, the spacing of the m gridlines is constant, Δn = constant.

4. *Meridional velocities.* A Runge-Kutta method solves Equations 4 and 5 for $c_m(n)$ along each n gridline and fills the field of the through flow component $c_m(m,n)$. For this initial value task, the initial values of $c_m(n_o)$ are adapted iteratively until the integral $\int_o^i c_m(n) \cdot \rho(n) \cdot dA_m$ matches the desired mass flow. For the first walkthrough, a linear interpolation in the n direction gives the local values of curvature $K(n)$ and inclination $\varepsilon(n)$ of the streamlines. For the next walkthroughs, $K(n)$ and $\varepsilon(n)$ result from step 5.

   First $c_m(n)$ is calculated at the inlet of the pre-runner using Equation 4 and assuming swirl free inflow with $c_{u1}' = 0$. Second $c_m(n)$ is calculated at the outlet of the pre-runner using Equation 5. β_{2o}' results from c_{m2o}' and c_{u2o}', where c_{u2o}' results from $\iota_o = 0$, assuming constant angular momentum between the impellers, $c_{u2o}' = c_{u1} \cdot r_{1o}/r_{2o}'$. The blade angle β_{B2o}' follows from $\Delta\beta_{2o}'$ and with ε_{2o}' also $\beta_{B2ax'o}$ is determined as well with Equation 3, $\beta_{B2ax}'(r_R)$. Analog $\beta_{B1ax}'(r_R)$ follows from β_{1o}', ε_{1o}', and ι_o'. Hence, the shape of the pre-runner blading described by Equations 1 through 3 is created. Now, with fixed $\beta_{B1ax}'(r_R)$ and $\beta_{B2ax}'(r_R)$, the calculation restarts at the inlet of the pre-runner and goes through every n gridline solving Equation 4 in the vaneless regions before and after the impellers as well as in the region $r > r_S$ of the main runner. Equation 5 solves for the remaining regions of the impellers.

5. *Streamlines.* Knowing the field $c_m(m,n)$ the spacing of the streamlines is corrected to equal mass flows between them. That alters the coordinates (z, r) of the grid points along the n gridline. Now B-splines of the fourth degree interpolate these new points, represent the streamlines, and give local values of curvature $K(m,n)$ and inclination $\varepsilon(m,n)$. Weighted averaging in the n direction of these values with its ancestor and descendant gives very natural distributions and helps the algorithm to convert very fast. Values at the inner and outer diameter stay unchanged.

6. *Meridional velocities.* With the updated values $K(m,n)$ and $\varepsilon(m,n)$ and the corrected grid, step 4 is repeated to obtain consistency of data. By optional repetition of steps 5 and 6, the results convert further, but for preliminary design, that is not necessary since the changes are usually very insignificant.

7. *Relative velocities on blades.* The calculation of the relative velocities on the blades goes back to the idea of Stanitz and Prian (1951) and is expressed by Equation 9.

$$w_{S,P} = \frac{\pi}{N} \cdot \sin\beta_B \cdot \frac{d(r \cdot c_u)}{dm} \pm 2\pi \cdot n \cdot \delta_B \cdot \sin\varepsilon \qquad (9)$$

8. *Output.* Changing an input value runs the full code and produces a complete preliminary result. The output is numerical and graphical.

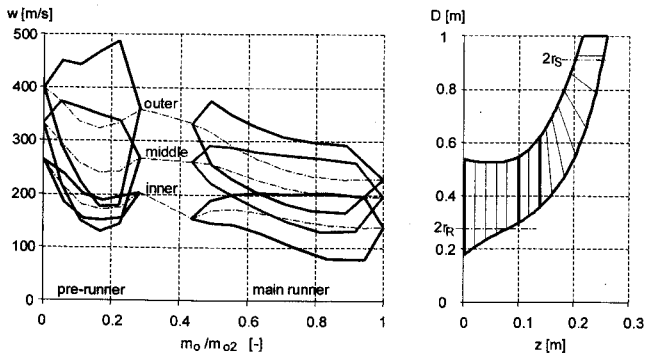

Figure 7 Design example.

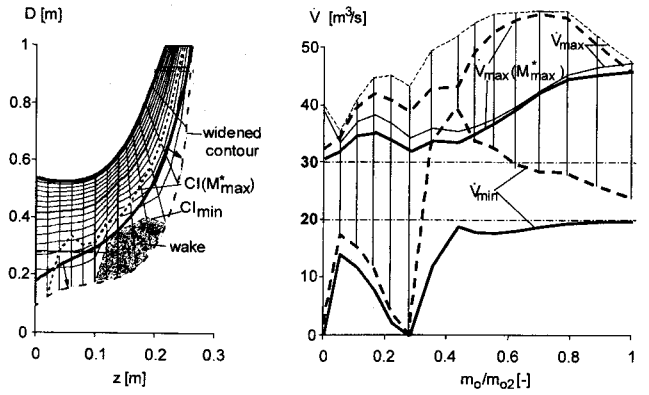

Figure 8 Flow stability and volume flow.

Off-Design Points. The blade angles $\beta_{B1ax}'(r_R)$ and $\beta_{B2ax}'(r_R)$ can be fixed, which goes around the blade generation in step (4). Changing the tip speeds, suction volume flow, or suction pressure and temperature then simulates off-design points. The inputs η', η, $\Delta\beta_{2o}'$, $\Delta\beta_{2i}'$, and μ_2 can be adjusted at the same time according to the judgment of the designer.

Design Example

The design example (Figure 7) shows that a reasonable design of pre-runner and main runner with radial-line blading is possible. The intended high-pressure ratio results in a compact system with high flow density and velocities close to the speed of sound. The results of the example correspond to practical experience.

The working fluid is water vapor under vacuum. The tip diameter of the main runner is to be 1 m (39.37 in.), the maximum tip speed is not allowed to exceed 500 m/s (1640 ft/s), and a suction volume flow of 30 m^3/s (1060 ft^3/s) at the highest rpm is assumed. The assumed efficiency is 70% in both impellers. Furthermore, a wide volume flow working range without flow instabilities is desired. Deceleration of the relative velocities should be acceptable.

Figure 7 (right) shows the meridional contour of the design example, and Figure 7 (left) shows the relative velocities on the blades. The deceleration ratios of these relative velocities are listed in Table 3. They all are within the limits with a certain safety margin. The safety margin is kept because of the low Reynolds numbers in the operating range, so no flow separation is expected.

TABLE 3
Deceleration Ratios of Relative Velocities

	Pre-runner				Main runner		
Criteria	w_2/w_1	w_{max}/w_2	w_{min}/w_1	Df	w_2/w_1	w_{max}/w_2	w_{min}/w_1
o.k. if	>0.75	<1.8	>0.3	<0.45	>0.6	<1.8	>0.3
outer	0.90	1.36	0.44	0.37	**0.69**	**1.64**	**0.50**
middle	0.81	**1.40**	**0.39**	**0.41**<0.6	0.76	1.48	0.50
inner	**0.77**	1.30	0.57	0.31<0.55	0.92	1.45	0.52

The shapes of the *w* curves correspond widely to the criteria of Dallenbach (1961). The local peaks at the outer diameter of the pre-runner are tolerated, since they vanish at the next streamline close to the outer diameter (not shown in Figure 7). Typical for such a design is the high loading at the outer diameter of the pre-runner and the relatively even distributed loading at the main runner.

Figure 3 shows how the load distribution changes with the change of the reference radius r_R for fine tuning. Large r_R shifts the loading more to the leading edge and small r_R shifts the loading toward the trailing edge. However, for large changes, the meridional contour has to be changed.

The working range of the design example lies in the range of 30 ... 20 m^3/s (1060 ... 705 ft^3/s), shown by the bold solid lines in Figure 8 on the right. The thin solid line shows where full blockage occurs, and the bold curve for $\dot{V}_{max}(M^*_{max})$ shows where the set Mach number limits of 1.3 in the absolute system or 1 in the relative system are reached. The doted inner contour $CI(M^*_{max})$ (Figure 8 on the left) roughly shows to what extent the contour can be narrowed until the Mach number limits are reached. At volume flows less then the minimum flow $\dot{V}_{min}$, instabilities occur due to force imbalance. Factors that help lower the minimum necessary volume flow are (1) lower curvature at the inner diameter, (2) higher curvature at the outer diameter, or (3) higher hub-tip ratios.

Flow Stability

Figure 8 also shows the effect of extended instabilities. For that purpose the hub-tip ratio of the example here is decreased by lowering the inner diameter (dashed contour in Figure 8). That leads to an imbalance in the force equilibrium, so that this region is considered as a wake region, where the flow is separated from the hub. This region is enclosed by the inner diameter and the inner contour with the minimum diameter required for the force equilibrium CI_{min}.

The physical background for the instabilities is further investigated in Müller (1999). They are due to higher total enthalpy at the outer radius and the resulting higher total pres-

sure there. To compensate this gradient from outer to inner diameter, a high gradient of the meridional velocity is needed since that controls the local pressure. High circumferential velocity components at high swirl ratios μ also help. But if the meridional velocity at the outer diameter is not high enough, the meridional velocity reaches zero above the inner diameter. Negative values for the meridional velocity (backflow) cannot solve the problem because they lower the local pressure in the same way as increasing positive values do. Thus, the forces cannot be balanced.

Müller (1999) uses a model. Assuming an axial flow in a pipe with solid-body swirl distribution $c_u(r)/r = \omega \cdot \mu$ and a equivalent distribution of total enthalpy $h_t(r) = h_{t1} + c_u(r) \cdot \omega \cdot r$, the closed solution for the simple radial equilibrium of forces gives the distribution $c_m(r)$ relative to c_{mo} at the outer diameter:

$$\frac{c_m}{c_{mo}}\left(\frac{r}{r_o}\right) = \sqrt{1 - \frac{2 \cdot \mu \cdot (\mu - 1) \cdot \left(\left(\frac{r}{r_o}\right)^2 - 1\right)}{\frac{c_{mo}}{u_o}}} \qquad (10)$$

For the ratios $r/r_o < (r_i/r_o)_{min}$ occurring only at $\mu < 1$ and $c_{mo}/u_o < 0.707$, there is no real solution; c_m reaches zero at $(r_i/r_o)_{min}$. The minimal ratios $(r_i/r_o)_{min}$—interpreted as hub-tip ratios—are shown in Müller (1999). They reach their maximum at a swirl ratio of 0.5, which mostly is reached halfway in the pre-runner, but curvature and inclination of the streamlines in a compressor shift the critical region toward the inlet of the main runner.

Design Rules

Müller (1999) derives design rules by applying Euler's equation to a mean line model and substituting parameters so that only chosen design parameters remain.

$$\tilde{e}_{com} = \mu_2 \cdot u_2^2 + \mu_1 \cdot D_1^2 \cdot \left(\pi \cdot n' \cdot \frac{u_2}{D_2} - \left(\frac{u_2}{D_2}\right)^2\right) \qquad (11)$$

The evaluation of Equation 11 easily shows that for maximum work transmission in such a design (1) the tip speed μ_2 and (2) inlet diameter D_1 of the main runner and (3) the number of revolutions of the pre-runner n' should be chosen to be maximum. The same is true for the (4) deviation coefficient μ_2 and the (5) pre-swirl coefficient μ_1 of the main runner, but generally there is not much room to maneuver these parameters. (6) Furthermore, the rpm of the main runner should be double that of the pre-runner if the pre-swirl ratio is $\mu_1 = 1$ or otherwise $n'/n = 1 + \mu_1$. Müller (1999) also gives an approximate relationship for the best inlet diameter at the pre-runner inlet for which the highest suction volume flow is obtained without exceeding given Mach number limits:

$$D'_{1o\,opt} = \frac{D'^2_{1i}}{3} + \frac{2}{3} \cdot \frac{M^{*2}_{wmax} \cdot \frac{2\kappa}{\kappa + 1} \cdot G \cdot T'_{tc1}}{(\pi \cdot n')^2 \cdot \left(1 - \frac{\kappa - 1}{\kappa + 1} \cdot M^{*2}_{wmax}\right)} \qquad (12)$$

In the same investigation, Müller shows that with a pre-runner instead of an inducer, the work transmission can be increased by 15...40% and using a pre-runner instead of a stator by 40 ... 120% depending mainly on the ratio D_1/D_2. The low values are for $D_1/D_2 = 0.4$ and the high values for $D_1/D_2 = 0.6$.

DISCUSSION

The algorithm introduced here shows a closed procedure for a complete preliminary design of compressors consisting of pre-runner and main runner, but assumptions such as the efficiency coefficients remain and must be handled with proper judgment by the designer. The algorithm is also suitable for transonic regions, but, it must be emphasized, no supersonic shocks are considered. The advantages of the algorithm are its robustness, speed, and ease of use, which allow it to be easily adapted to other flow-calculation tasks as long as they are restricted to radial-line blading. Regions before the pre-runner and after the main-runner can easily be included also using Equations 4 and 5.

CONCLUSIONS

This study demonstrates the possibility of designing a compressor consisting of separately driven pre-runner and main runner. The algorithm introduced is fast, universal, and simple for preliminary design and flow calculation. It allows instantaneous design and analysis of different geometries; therefore, it can be used as an initial step in a design process where currently available CFD impeller analysis codes would be much more time consuming. Although the system investigated here consists of an axial pre-runner with curved blades and a mixed-flow main runner with straight blades, the algorithm can easily be adapted to any system that may consist of axial, mixed, and radial-flow impellers and stationary guide vanes, as long as they have radial-line blading.

In this quasi-three-dimensional code, a blade-to-blade flow calculation is superimposed on a two-dimensional throughflow calculation. The algorithm is not restricted to a free vortex distribution. It is primarily based on the equilibrium of forces and the satisfaction of continuity. Losses and viscous effects are introduced by means of efficiency coefficients. The intended application was the compression of water vapor under a vacuum condition with a high pressure ratio for use in an environmental friendly refrigeration plant with water as a refrigerant.

ACKNOWLEDGMENTS

I especially thank E. Linder, Ph.D., Professor, Department of Mechanical Engineering, Technische Universität, Dresden, Germany (now retired) for his encouragement and

support. I would like to thank R. Pauer, Ph.D., and J. Klingenberg, Ph.D., Department of Mechanical Engineering, Technische Universität, Dresden, Germany, for their discussion and practical support. The idea of the work was inspired by the daily demands of research at Institut für Luft- und Kältetechnik (ILK), Dresden gGmbH, Germany, where I worked three years as a research officer. So with great respect I want to mention the ambition, endurance, and skills of my colleagues there.

NOMENCLATURE

c = absolute velocity, m/s
D = diameter, m
Df = diffusion factor, $1-w_2/w_1 + 0.5 \cdot t/L \cdot (w_{u1}-w_{u2})/w_1$
e = specific shaft work, J/kg
G = gas constant, J/kgK
h = specific enthalpy, J/kg
K = curvature, m^{-1}
L = cord length, m
L_{ax} = axial length, m
m = coordinate in meridional direction, m
$\dot{m}$ = mass flow, kg/s
M^* = critical mach number
n = number of revolutions, s^{-1}
n = coordinate in n direction, m
N = blade number
p = pressure, Pa
r = radius, m
r_R = reference radius, m
r_S = Stanitz radius, Equation 6, m
t = pitch, m
T = temperature, K
u = circumferential velocity of impeller, m/s
$\dot{V}$ = volume flow, m^3/s
w = relative velocity, m/s
z = coordinate in axial direction, m
α = flow angle in absolute system, °
β = flow angle in relative system, °
$\bar{\gamma}$ = stagger—angle of cord line measured from circumferential direction, °
Δ = difference
δ = blade thickness, m
ε = inclination angle, °
ε_n = inclination angle of n direction, °
η = efficiency coefficient
ι = incidence angle, °
κ = isentropic exponent
μ = swirl ratio c_u/u
μ_2 = deviation coefficient, here defined as c_{u2}/u_2 for $\beta_{B2}=90°$
Θ = angle in circumferential direction, °
ρ = density, kg/m^3
ω = angular speed, s^{-1}

Subscript

ax = velocity component in axial direction; angle measured from axial direction (not from meridional direction)
B = blade
c = in absolute system
C = circle
com = combined (pre-runner and main runner together)
i = inner diameter
o = outer diameter
opt = optimum
m = velocity component in *m* direction (meridional direction)
max = maximum allowed
min = minimum required
r = velocity component in radial direction
s = suction side on blades
t = total value (measured at stagnation point)
u = velocity component in circumferential direction
w = in relative system
1 = inlet
2 = outlet

Superscript

‘ = pre-runner

REFERENCES

Albring, P., and N. Müller. 1995. Turboverdichter für Wasser als Kältemittel. In W. Faragallah and D. Surek, *Beiträge zu Fluidenergiemaschinen*, Band 2, pp. 16-22. Sulzbach: Verlag und Bildarchiv W.H. Faragallah.

Albring, P., R. Apley, B. Burandt, and N. Müller. 1998. Grundlagenuntersuchungen energierationeller Kreisprozesse mit Wasser als Kältemittel und Erprobung einer Versuchs-Großanlage. Abschlußbericht zum BMBF-Forschungsvorhaben 0326921A.

Albring, P., R. Apley, B. Burandt, K. Döge, G. Heinrich, E. Lindner, N. Müller, R. Pauer, R. Pilling, and R. Rudischer. 1994. Turbo-compressor impeller for coolant, United States Patent No. 5,464,325.

Busemann, A. 1928. Das Förderhöhenverhältnis radialer Kreiselpumpen mit logarithmisch-spiraligen Schaufeln. ZAMM 8, pp. 372-374.

Dallenbach, P. 1961. The aerodynamic design and performance of centrifugal and mixed-flow compressors. SAE-Paper No. 268A.

Farin, G. 1993. *Curves and surfaces for computer aided geometric design: A practical guide*. New York: Academic press.

Lieblein, L. 1965. In *Aerodynamic design of axial-flow compressors*, I.A. Johnson and R.O. Bullock. Washington, D.C.: NASA-Administration.

Müller, N. 1999. Entwurf von Laufrädern mit Radialfaserschaufeln für Diagonalverdichter mit getrennt angetriebenen Vorläufer und Hauptläufer. Dissertation, Technische Universität Dresden.

Traupel, W. 1988. *Thermische Turbomaschinen*. Band 1. Berlin: Springer.

Schmitz, F.W. 1960. *Aerodynamik des Flugmodells*. Duisburg: Verlag Lange.

Stanitz, J.D., and V.D. Prian. 1951. A rapid approximate method for determining velocity distributions on impeller blades of centrifugal compressors. NACA - TN 2421.

Weinig, F. 1935. *Die Strömung um die Schaufeln von Turbomaschinen*. Leipzig: Verlag Barth.

Wennerstrom, A.J. 1965. Simplified design theory of highly loaded axial compressor rotors and experimental study of two transonic examples. Dissertation, ETH Zürich.